Helminth-derived metabolites induce tolerogenic functional, metabolic, and transcriptional signatures in dendritic cells that attenuate experimental colitis

Nathalia L. Malacco[1]*, Aubrey N. Michi[2,3]*, Elizabeth Siciliani[1], Ana G. Madrigal[1], Tamara Sternlieb[1], Ghislaine Fontes[4], Irah L. King[4], Igor Cestari[1], Armando Jardim[1], Mary M. Stevenson[1,4], Fernando Lopes[5]

[1]Institute of Parasitology, McGill University, Ste-Anne-de-Bellevue, QC, H9X 3V9, Canada
[2]Department of Cancer Biology, Dana-Farber Cancer Institute, Boston, MA, 02215, USA
[3]Department of Cell Biology, Harvard Medical School, Boston, MA, 02215, USA
[4]Department of Microbiology and Immunology, McGill University, Montreal, QC, H3A 2B4
[5]The Broad Institute of MIT and Harvard, Cambridge, MA, 02142, USA
***Equal contribution**

Correspondence: lopes@broadinstitute.org

Keywords: Tolerogenic dendritic cells, metabolites, metabolomics, transcriptomics, colitis

Summary Sentence: Metabolites produced by *Heligmosomoides polygyrus* induce metabolic and transcriptional changes in DCs consistent with tolDCs, and adoptive transfer of these DCs attenuated DSS-induced intestinal inflammation.

ABSTRACT

Inflammatory bowel diseases (IBD) are chronic inflammatory diseases in which abdominal pain, bloody diarrhea, weight loss, and fatigue collectively result in diminished quality of patient life. The disappearance of intestinal helminth infections in Western societies is associated with an increased prevalence of IBD and other immune-mediated inflammatory diseases. Evidence indicates that helminths induce tolerogenic dendritic cells (tolDCs), which promote intestinal tolerance and attenuate intestinal inflammation characteristic of IBD, but the exact mechanism is unclear. Helminth-derived excretory-secretory (HES) products including macromolecules, proteins, and polysaccharides have been shown to modulate the antigen presenting function of DCs with down-stream effects on effector $CD4^+$ T cells. Previous studies indicate that DCs in helminth-infected animals induce tolerance to unrelated antigens and DCs exposed to HES display phenotypic and functional features of tolDCs. Here, we identify that nonpolar metabolites (HnpM) produced by a helminth, the murine gastrointestinal nematode *Heligmosomoides polygyrus bakeri* (Hpb), induce tolDCs as evidenced by decreased LPS-induced TNF and increased IL-10 secretion and reduced expression of MHC-II, CD86, and CD40. Furthermore, these DCs inhibited OVA-specific $CD4^+$ T cell proliferation and induced $CD4^+Foxp3^+$ regulatory T cells. Adoptive transfer of HnpM-induced tolDCs attenuated DSS-induced intestinal inflammation characteristic of IBD. Mechanistically, HnpM induced metabolic and transcriptional signatures in BMDCs consistent with tolDCs. Collectively, our findings provide groundwork for further investigation into novel mechanisms regulating DC tolerance and the role of helminth secreted metabolites in attenuating intestinal inflammation associated with IBD.

45 **INTRODUCTION**

46 Inflammatory bowel diseases (IBD) such as Crohn's disease and ulcerative colitis (UC) are
47 characterized by symptoms of watery or bloody diarrhea, abdominal pain, fatigue, weight loss, and
48 significantly diminished patient quality-of-life[1, 2]. In genetically-prone individuals,
49 environmental factors contribute to dysregulated intestinal tolerance, leading to immune responses
50 to foreign antigens that are usually innocuous[3]. This dysregulated tolerance results in
51 exaggerated $CD4^+$ Th_1 and Th_{17} cell responses[4-8], and, in some cases, atypical Th_2 responses[9,
52 10].

53 Evidence indicate that a broad range of helminth species induce intestinal tolerance and inhibit
54 intestinal inflammation by modulating $CD4^+$ Th cell responses. In particular, lamina propria (LP)
55 T cells from wild-type (WT) C57Bl/6 (B6) mice infected with *Heligmosomoides polygyrus bakeri*
56 (Hpb), a murine gastrointestinal nematode, secrete high levels of the regulatory cytokines IL-10
57 and TGF-β[11]. Furthermore, T cells from the mesenteric lymph nodes (MLN) of Hpb-infected
58 WT B6 mice alleviate established intestinal inflammation when transferred into IL-$10^{-/-}$
59 recipients[12]. Interestingly, Hpb infection mitigates the Th_1/Th_{17}-driven intestinal inflammation
60 observed in IL-$10^{-/-}$ mice[12, 13]. Infections with various helminth species including Hpb also
61 protect mice from chemically induced intestinal inflammation[13-18].

62 $CD4^+$ Th cell responses are shaped by antigen presenting cells (APCs) especially dendritic
63 cells (DCs), which also promote immune tolerance by influencing $CD4^+$ T cell responses via
64 inducing T cell depletion, T cell anergy, and regulatory T cells (T_{regs})[19, 20]. A potential
65 mechanism by which helminths indirectly shape $CD4^+$ Th cell responses is by their ability to
66 modulate DC function. Importantly, monocyte-derived DCs from patients with helminth
67 infections[21] and DCs from mice with experimental helminth infections induce tolerance to

68 unrelated antigens[22]. Moreover, helminths release molecules that shift DCs toward a tolerogenic
69 DC (tolDC) phenotype, which modulate $CD4^+$ Th cell polarization and inhibit experimental
70 intestinal inflammation[23-25]. Helminth-derived products induce distinct DC phenotypes in
71 terms of co-stimulatory molecule expression, cytokine production, and signaling pathways[25-27].
72 Thus, it is critical to identify molecules in the helminth secretome and characterize their
73 immunomodulatory effects, especially their ability to induce novel tolerogenic pathways. Previous
74 studies have identified important phenotypic and functional changes in DCs and macrophages in
75 response to secretome components, including macromolecules, proteins, and polysaccharides, of
76 various helminths. Here, we investigated the responses of DCs to metabolites in the excretory-
77 secretory products of Hpb adult worms by characterizing the functional, metabolic, and
78 transcriptional signatures of DCs treated with Hpb-derived metabolites. We also determined the
79 effects of these DCs on $CD4^+$ Th cell responses *in vitro* and their therapeutic effects *in vivo* on
80 experimental colitis in mice induced by administration of DSS, a widely used method to induce
81 intestinal inflammation.
82

83 **RESULTS & DISCUSSION**

84 **Hpb-derived non-polar metabolites (HnpM) induce a tolerogenic DC phenotype**

85 Engagement of TLR4 expressed on DCs by bacterial lipopolysaccharide (LPS) initiates a
86 complex signaling cascade and the release of proinflammatory cytokines including TNF, IL-6, IL-
87 8, and IL-1β[28]. To investigate if helminth-derived metabolites induce tolDCs, we isolated polar
88 (HpM) and nonpolar (HnpM) metabolites from Hpb culture supernatants using chromatography.
89 We first questioned if HpM and HnpM metabolites induce a tolerogenic phenotype in DCs by
90 determining changes in proinflammatory and immunoregulatory cytokine secretion. Bone

91 marrow-derived DCs (BMDC) were prepared from B6 mice and cultured in the presence of HnpM
92 or HpM for 20 h and stimulated subsequently with 100 ng/ml LPS for 4 h **(Fig. 1a)**. Mock purified
93 polar and non-polar fractions from media without Hpb were used as negative controls. As
94 expected, LPS induced BMDC to secrete high levels of TNF **(Fig. 1b)**. Remarkably, TNF
95 production was significantly reduced when BMDCs were incubated with HnpM compared to LPS
96 alone, the HpM fraction, or polar/nonpolar controls. BMDCs treated with HnpM and stimulated
97 with LPS had significantly enhanced IL-10 production compared to LPS alone; there were no
98 changes in IL-10 production by BMDCs pre-treated with HpM or polar/nonpolar controls **(Fig.
99 1b)**. It should be noted that in the absence of LPS stimulation, neither HpM nor HnpM altered
100 BMDC secretion of TNF or IL-10 (data not shown). The TNF/IL-10 ratio was more than 2-fold
101 higher in HnpM-treated compared to control BMDCs after LPS stimulation **(Fig. 1c)**. Together,
102 these data suggest that HnpM present in HES produced by Hpb induced a cytokine profile in
103 BDMCs characteristic of tolDCs. There are conflicting reports regarding the ability of helminth
104 products to modulate TLR-dependent pathways in DCs. For instance, *Schistosoma mansoni*
105 soluble egg antigen has been shown to suppress MyD88-dependent and independent pathways
106 leading to IL-12p40 production induced by engaging TLR3, TLR4, or TLR9[29]. We have shown
107 previously that unfractionated HES from Hpb suppresses IL-12p70 as well as IL-10 secretion by
108 BMDCs following TLR4 or TLR9 ligation[23]. Thus, it is likely that different helminth species
109 secrete various molecules that have diverse effects on DC cytokine secretion and other functions.
110 In addition to cytokines produced by antigen presenting cells (APC) including DCs, activation
111 of $CD4^+$ T cells as fully licensed effector cells requires T cell receptor (TCR) signaling initiated
112 by binding to cognate peptide-MHC complexes expressed by DCs and co-stimulatory molecule
113 expression. TolDCs are known to express low levels of MHC complexes and co-stimulatory

114 molecules[30]. BMDCs pre-treated for 20 h with HnpM had significantly reduced expression of
115 MHC-II and the co-stimulatory molecules CD86 and CD40 **(Fig. 1d, 1e)**. Moreover, CD11c$^+$ DCs
116 isolated from the spleens of mice treated i.p. with HnpM once daily for 3 days also had reduced
117 expression of MHC-II, CD86, and CD40, an observation that corroborates our *in vitro* findings in
118 BMDCs treated with HnpM **(Fig. 1f, 1g)**.

119 To functionally assess the tolerogenic capacity of DCs treated *in vitro* with HnpM, we
120 investigated if these DCs inhibited antigen-specific CD4$^+$ T cell proliferation using the OT-II
121 transgenic mouse model. HnpM-treated DCs were pulsed with OVA or the OT-II peptide 323-339
122 for 6 h and co-cultured with purified CFSE-labelled OT-II CD4$^+$cells for 72 h. HnpM-treated DCs
123 signifantly suppressed OVA-specific CD4$^+$ T cell proliferation **(Fig. 1h-1j)**. In addition, CD4$^+$ T
124 cells co-cultured with HnpM-treated DCs displayed increased polarization towards Treg cells that
125 expressed Foxp3 **(Fig. 1k, 1l)**.

126

127 **HnpM induce metabolic changes in DCs**

128 Since metabolic reprogramming of immune cells is closely intertwined with inflammatory and
129 tolerogenic responses, we next sought to determine if a unique metabolic signature distinguishes
130 HnpM-induced tolDCs. We performed untargeted metabolomics on supernatants harvested from
131 BMDCs treated with PBS or HnpM for 4 and 20 h **(Fig 2a)**. As the identity and chemical
132 composition of most host metabolites are still undefined, our aim was to identify a comprehensive
133 molecular weight profile of HnpM-treated DCs to pinpoint potentially new metabolite biomarkers.
134 Using this unbiased approach, we observed that supernatants harvested from BMDCs treated with
135 HnpM contained 1,992 unique metabolite peaks **(Sup. File)**. To create a hierarchy of relevant
136 metabolic changes, the peaks were selected using a 2-fold change cut-off against cell-free media

137 control samples, in which 227 peaks were identified **(Sup. File)**. Data were analysed using
138 MetaboAnalyst; interquartile range (IQR) filtering reduced the number of peaks to 225 in the
139 supernatants of HnpM-treated DCs. Principal component analysis (PCA) indicated that BMDCs
140 treated with HnpM for 4 h formed clusters distinct from control BMDCs **(Fig. 2c)**. Curiously, DCs
141 that were exposed to HnpM for 20 h clustered together independently of pre-treatment with HnpM.
142 Moreover, a similar pattern was observed by heatmap analysis of peaks clustered by similarity
143 **(Fig. S1a, S1b)**.

144 As the metabolite analysis of DCs treated with HnpM for 20 h did not reveal meaningful
145 differences, we pursued further analysis focusing on the 4 h group. Statistical analyses indicated a
146 downregulated clustering of metabolites **(Fig. S1c)** as shown in the heatmap of the top 50 most
147 enriched metabolites **(Fig. 2b)**. Volcano plot analysis showed a total of 17 downregulated
148 metabolites, as opposed to only one upregulated metabolite of the 225 total peaks analyzed **(Fig.
149 S1d)**. Functional analyses were performed to infer pathways related to the differentially enriched
150 metabolites by using Mummichog enrichment and KEGG database. The results predicted a total
151 of 29 pathways and 43 matched compounds **(Sup. File)**. Scatter plot test of significant peaks
152 revealed two differentially enriched pathways: sphingolipid metabolism and terpenoid backbone
153 metabolism with the metabolite, C00418, a potential match to mevalonic acid (3,5-dihydroxy-3-
154 methylvaleric acid), according to the KEGG compound database **(Fig. 2d)**. Interestingly,
155 sphingolipid metabolism has been associated with the resolution phase of inflammatory responses
156 in human macrophages as shown by sharp increases in glycosphingolipids and cholesteryl esters
157 during this phase[31]. Furthermore, sphingolipid metabolism is essential for DC activation and
158 secretion of pro-inflammatory cytokines in response to stimulation by TLR ligands[32]. In
159 particular, the mevalonate pathway has been implicated in DC maturation as evidenced by

160 increased expression of MHC class II and CD40 by DC and increased cytokine production[33].
161 Together, these data support the conclusion that the metabolic profile induced in DCs by treatment
162 with HnpM is consistent with HnpM interference in DC activation leading to polarization of DCs
163 to a tolerogenic phenotype.
164

165 **HnpM induce a unique transcriptomic signature in DCs**

166 Previous studies have shown that immunogenic DCs and tolDCs express distinct
167 transcriptional profiles[34, 35]. Using matched samples of DCs from the metabolomic study, we
168 compared the transcriptional profiles of HnpM-treated and control DCs at 4 and 20 h using RNA
169 sequencing **(Fig. 2a)**. Differential expression analysis of HnpM-treated BMDCs against control
170 samples showed that DCs treated with HnpM for 4 h did not present any statistically significant
171 changes in gene expression **(Fig. S2a)**. Conversely, DCs treated with HnpM for 20 h had 183
172 significantly upregulated and 76 significantly downregulated genes **(Fig. 3a, 3b; Sup. File)**. The
173 differences in the metabolome at 4 h and changes in gene expression at 20 h suggest that HnpM
174 initially induced a metabolic shift that does not require gene regulation, that is, the metabolic shift
175 preceded HnpM-induced changes in gene expression. Indeed, previous studies indicate that
176 metabolism may regulate gene expression. DNA and histones are modified by different
177 modulators, such as histone-modifying enzymes, chromatin-remodelling complexes, and
178 transcription regulators. The enzymatic activities of these modifiers are regulated by metabolism
179 via production of metabolites and metabolic enzymes[36]. Thus, the changes in metabolites and
180 gene expression that we observed in HnpM-treated BMDCs may be important signatures of tolDCs
181 induced by metabolites produced by Hpb and other helminths.

182 Gene ontology (GO) annotation and pathway enrichment ontology clusters with network
183 layouts of representative terms of the upregulated genes revealed statistically enriched terms,
184 showing significant features associated with immune responses, including exogenous antigen
185 processing and presentation, cell signaling, and regulation of cytokine production as well as the
186 adaptive immune response **(Fig. 3c; Sup. File)**. The protein-protein interactions (PPI) and
187 MCODE algorithms were applied to this network to identify neighborhoods where proteins are
188 densely connected. This analysis strongly confirmed features related to exogenous antigen
189 presentation by MHC-II **(Fig. S2b, S2c)**. Enrichment ontology clusters and network layouts for
190 the downregulated genes showed significance in genes related to cell proliferation, including
191 mitotic cell cycle and cytokinesis **(Fig. 3d, Fig. S2d-S2g, and Sup. File)**.

192 GSEA analysis revealed that the differentially expressed genes identified in BMDCs treated
193 with HnpM had significant similarities with genes previously identified to be upregulated in
194 dexamethasone-[37] and vitamin D3-induced[38] tolDCs **(Fig. 3e, Fig. S2h, S2i, Supp. File)**. Of
195 note, there were common genes in the barcode leading-edge genes (**Sup. File**). Upregulated genes
196 identified in our transcriptomics and enrichment ontology clusters indicated these genes are
197 involved in regulating the inflammatory response **(Fig. S2j)**. Moreover, integrative analysis of
198 transcriptional and metabolic signatures showed relevant and statistically significant pathways
199 related to the regulation of immune responses, including antigen processing and presentation,
200 differentiation of Th_1 and Th_2 cells, D-arginine and D-ornithine metabolism, and the PI3K-Akt
201 signaling pathway **(Fig. 3f and Sup. File)**. Previous studies showed that subsets of DCs have
202 molecular signatures including those involved in immune system processes, cell differentiation,
203 metabolism, and cell death which are associated with their activation status. For example, the
204 expression of critical genes, such as macrophage galactose N-acetyl-galactosamine (*Mgl2)*,

205 cadherin-1 (*Cdh1*), CD137 (*TNF-asf9*), and RhoB (*RhoB*) were observed to change markedly with
206 DC maturation[39]. Of note, our GSEA analysis displayed remarkable similarity in HnpM-treated
207 DCs to differentially expressed genes in tolDCs. Together, these findings may lead to the
208 identification of a helminth-induced tolerogenic transcriptional signature in DCs and expand our
209 understanding of the interactions between the helminth secretome and host immune tolerance.
210

211 **Adoptive transfer of HnpM-treated DCs alleviates intestinal inflammation in experimental**
212 **colitis**

213 Recently, progress in the development of pharmaceutical strategies to attenuate intestinal
214 inflammation characteristic of IBD has been noteworthy including immunosuppressive therapies,
215 such as anti-cytokine monoclonal antibodies, and antibiotic therapy to control microbiota species
216 and abundance[45,46]. Importantly, there is no available treatment to date to rescue or induce
217 tolerance to alleviate intestinal inflammation and modulate disease severity. As described above,
218 TNF secretion by HnpM-treated BMDC was significantly decreased *in vitro* in response to LPS
219 stimulation together with increased IL-10 production. We also observed that exposure of DCs *in*
220 *vitro* or *in vivo* to HnpM resulted in reduced expression of MHC-II and co-stimulatory molecules
221 by BMDCs and splenic DCs, respectively. Co-culture of HnpM-treated BMDCs dramatically
222 reduced OVA-specific $CD4^+$ T cell proliferation and increased the frequency of $Foxp3^+$ Tregs.
223 These observations prompted us to investigate the tolerogenic potential of HnpM-treated BMDCs
224 in mice with DSS-induced intestinal inflammation. B6 mice administered 3% DSS in drinking
225 water for 5 days[40] were injected i.p. with either 1 x 10^6 control BMDCs or HnpM-treated
226 BMDCs. Mice adoptively transferred with HnpM-treated DCs displayed significant reductions in
227 disease activity score (DAS), colon shortening, and weight loss **(Fig. 4a-4c)**. Histopathological

228 analysis indicated decreased loss of intestinal parenchyma and significantly less tissue damage in
229 the mid-distal colon **(Fig. 4d)**. We have previously reported that adoptively transferred
230 BMDCs[41] or macrophages[42] migrate to the spleen, MLN, and GI tract of recipient mice where
231 they can interact with T cells. In previous work, we confirmed that adoptively transferring
232 regulatory/tolerogenic APCs, such as macrophages, which migrate to secondary lymphoid organs
233 and interact with T cells to alleviate intestinal inflammation[42]. Others demonstrated that
234 adoptive transfer of tolDCs[43] effectively blocked dinitrobenzene sulfonic acid (DNBS)-induced
235 intestinal inflammation in immunocompetent mice. In contrast, adoptive transfer of tolDCs was
236 ineffective in $Rag^{-/-}$ mice with DNBS-induced colitis, indicating interaction between tolDCs and
237 T cells is critical to alleviate intestinal inflammation characteristic of IBD.
238

239 **CONCLUSION**

240 Tolerogenic DCs (tolDCs) promote immune homeostasis and tolerance by influencing $CD4^+$
241 Th cell responses via various mechanisms including inducing $Foxp3^+$ Tregs[19-22]. Recent studies
242 indicate that different functional classes of DCs are marked by distinct phenotypic, molecular and
243 transcriptional profiles, which translate to a diversity of immunological functions among DC
244 subsets. Collectively, our findings demonstrate that DC maturation and function are influenced by
245 exposure to HnpM produced by adult stage Hpb. Treatment with HnpM *in vitro* or *in vivo* induced
246 tolerogenic features in DCs including modulating their cytokine secretion in response to the TLR4
247 agonist LPS and expression of MHC-II, CD86, and CD40 responses associated with inhibition of
248 antigen-specific, effector $CD4^+$ T cell responses and induction of $Foxp3^+$ Tregs. Importantly,
249 adoptive transfer of HnpM-induced tolDCs resulted in dramatic reduction in intestinal
250 inflammation in DSS-induced colitis in mice. Mechanistically, HnpM induced metabolic and

transcriptional signatures in BMDCs consistent with those established previously for tolDCs[19, 20].

It is likely that metabolites and other molecules released by helminths, which promote tolDCs, have evolved as an immune evasion mechanism to avoid expulsion by the host and establishment of a chronic infection characteristic of these parasites. Thus, our findings provide groundwork for further investigation into novel mechanisms regulating DC tolerance and the role of helminth secreted metabolites in attenuating intestinal inflammation associated with IBD. Future studies may uncover novel pathways to induce tolDCs by harnessing information from the list of metabolites and genes regulated up or down by HnpM presented here, leading to innovative therapies to treat IBD and other immune-mediated, inflammatory diseases.

AUTHOR CONTRIBUTIONS

Conceptualization, N.L.M., A.N.M., A.J., M.M.S., F.L.; Data Curation, N.L.M., A.N.M., T.S., G.F., I.L.K., I.C., A.J., F.L.; Data Analysis, N.L.M., A.N.M., T.S., G.F., I.L.K., I.C., A.J., F.L.; Funding Acquisition, M.M.S., F.L.; Investigation, N.L.M., A.N.M., G.F., I.L.K.; Methodology, N.L.M., A.N.M., E.S., A.G.M., T.S., G.F., I.L.K., I.C., A.J., M.M.S., F.L.; Project Administration, F.L.; Resources, I.L.K., M.M.S., F.L.; Software, I.C.; Supervision, M.M.S, F.L.; Validation, F.L.; Visualization, N.L.M., A.N.M.; Writing - Original Draft, N.L.M., A.N.M.; Writing - Review & Editing, N.L.M., A.N.M., E.S., A.G.M, T.S., G.F., I.L.K., I.C., A.J., M.M.S., F.L.

ACKNOWLEDGEMENTS

We thank Dr. Judith Mandl (McGill University) for generously providing B6 OT-II mice. This study was supported by the Natural Science and Engineering Research Council of Canada (NSERC) (grant numbers RGPIN/04459-2019 to F.L. and RGPIN/1327730 to M.M.S.), Canadian Institutes Health Research (CIHR) (grant number MOP130369) to M.M.S., and Fonds de Recherche du Québec – Nature et Technologies (FRQ-NT) (grant number 253419) to M.M.S. and F.L.

278 **MATERIALS & METHODS**

279 **Mice** Male BALB/c mice, 8-10 weeks old, and female C57Bl/6 (B6) mice, 6-8 weeks old, obtained
280 from Charles River Laboratories (St. Constant, QC, Canada) and B6 OT-II/Rag$^{-/-}$ mice, 6-8 weeks
281 old, were housed under specific pathogen-free conditions at McGill University. All experiments
282 were approved and conducted in accordance with the guidelines of the Canadian Council on
283 Animal Care.

284 ***H. polygyrus bakeri* (Hpb)-Derived Metabolites** Helminth-derived excretory/secretory (HES)
285 products were obtained as previously described[44]. BALB/c mice were infected with 400-500
286 infective larvae (L3) of Hpb for 21 days. Adult worms were collected from the small intestine and
287 cultured in RPMI 1640 medium containing 2% w/v glucose, 80 μg/ml gentamicin, 100 U/ml
288 penicillin/streptomycin, and 20 μg/ml polymyxin B for 40 h at 37°C, 5% CO_2. Supernatant was
289 collected, centrifuged at 8000 × *g* for 10 min at 4°C, and passed through a 0.2 μm filter.
290 Metabolites were separated from proteins and exosomes using a 3 kDa MWCO centrifugation unit
291 (UFC910024, Millipore) and centrifuged at 4000 × *g* for 40 min at 4°C. Hpb-derived metabolites
292 were further separated into polar (HpM) and nonpolar (HnpM) fractions by chromatography using
293 a C_{18} column. The flow-through containing polar metabolites from the C_{18} column was further
294 subjected to a universal polymeric reversed-phase sorbent containing column (WAT106202,
295 Waters), and the polar metabolites were eluted using acetonitrile at 100% v/v. HpM and HnpM
296 stock fractions were concentrated using a speed vacuum concentrator, resuspended in ultrapure
297 water and maintained at -20°C.

298 **Dendritic Cells** Bone marrow-derived dendritic cells (BMDCs) and splenic dendritic cells (DCs)
299 were obtained from B6 mice. Bone marrow cell suspensions were cultured and differentiated in
300 10 cm petri dishes in complete RPMI 1640 medium supplemented with 10% fetal bovine serum

301 (FBS), 1% 100X penicillin/streptomycin solution, 1% 100 mM sodium pyruvate, and 20 ng/ml
302 GM-CSF (StemCell Technologies) for 8 days at 37°C, 5% CO_2. On days 3 and 6, BMDCs were
303 given an additional 10 ml and 5 ml, respectively, of complete medium containing 20 and 40 ng/ml
304 GM-CSF. Floating cells were collected and used for all experiments; flow cytometry confirmed
305 the purity of BMDCs as >90% $CD11c^+$. Aliquots of BMDCs (1×10^5) were seeded into 96-well
306 plates, treated with 50 μg/ml HnpM, 50 μg/ml HpM, or 50 μg/ml polar and nonpolar control mock
307 extractions in complete RPMI 1640 containing 20 ng/ml GM-CSF and cultured at 37°C, 5% CO_2
308 for 20 h, washed, and stimulated with LPS (100 ng/ml; Millipore-Sigma) for 4 h. For splenic DCs,
309 spleens were minced, passed through a 40 μm cell strainer to obtain single cell suspensions, and
310 red blood cells lysed using ACK lysis buffer (ThermoFisher).

311 **Cytokine ELISAs** Supernatants were collected from BMDCS for TNF (R&D Technologies) or
312 IL-10 (R&D Technologies) quantification. ELISAs were performed according to manufacturer's
313 instructions.

314 **Immunophenotyping** Cultured BMDCs or splenic DCs were treated with Fc block, and labeled
315 with the following antibodies from BioLegend for 30 min at 4°C: anti-CD45-PeCy7, -CD11c-
316 FITC), -MHC-II (I-A/I-E)-BV421, -CD40-PE, and -CD86-PerCP mAbs. To quantify $CD4^+Foxp3^+$
317 cells, spleen cells were stained with anti-CD4-FITC mAb (eBioscience), fixed, and permeabilized
318 using the Foxp3 staining kit (Invitrogen), and stained with anti-Foxp3-Alexa Fluor 488 mAb
319 (eBioscience) for 30 min at 4°C. Cells were acquired in Attune Nxt flow cytometer (ThermoFisher
320 Scientific) and analyzed using FlowJo software v.10.2 (Tree Star).

321 **OVA-specific $CD4^+$ T cell proliferation** To evaluate OVA-specific $CD4^+$ T cell proliferation,
322 spleens were harvested from naïve OT-II TCR-transgenic mice, and single cell suspensions were
323 prepared as described above. $CD4^+$ T cells were isolated using the EasySep Mouse $CD4^+$ T cell

324 Isolation Kit (StemCell Technologies) according to the manufacturer's instructions. BMDCs were
325 either untreated or treated with 50 μg/ml HnpM for 24 h prior to co-culture with OT-II $CD4^+$ T
326 cells. During the last 6 h of culture, BMDCs were pulsed with 250 μg/ml OVA (Sigma) or 10
327 μg/ml OVA peptide 323-339 (Sigma) at 37°C, 5% CO_2, prior to co-culture for 72 h with purified,
328 CFSE-labelled (eBioscience) OT-II $CD4^+$ T cells at a final T cell:BMDC ratio of 2:1. Cells were
329 collected and labelled with anti-CD4-FITC and anti-CD44-APC mAbs (BD Biosciences). Flow
330 cytometry was used to determine CFSE dilution in gated $CD4^+CD44^+$ cells (LSR Fortessa; BD
331 Biosciences); data were analyzed using FlowJo software.
332 **DSS Treatment** Female B6 mice at 6-8 weeks old were provided with 3% w/v DSS (MP
333 Biomedicals) in drinking water *ad libitum* for 5 days. On day 5, drinking water was changed to
334 normal drinking water and mice were injected i.p. with 1 x 10^6 vehicle control (PBS) DCs, naïve
335 DCs, or HnpM-treated DCs. Mice were weighed daily. On day 8, necropsies were performed and
336 colon lengths, percent weight changes and disease activity scores (DAS) based on a scale of 0-5
337 were determined as previously described[45].
338 **Histology** Mid-distal colon sections were fixed in 10% neutral buffered formalin, embedded in
339 paraffin wax, and sectioned to 4 μm thickness. Sections were de-paraffinized in two changes of
340 xylene and rehydrating through graded ethanol solutions (100%, 95%, 70% EtOH) and distilled
341 H_2O. Sections were stained in Gills II hematoxylin (Leica Biosystems) for 5 minutes and rinsed in
342 warm tap water for 5 minutes and counter-stained in eosin (Leica Biosystems) for 1 min followed
343 by 1 min in distilled H_2O. Slides were dehydrated through reverse graded ethanol solutions (70%,
344 95%, 100% EtOH) and cleared in two changes of xylene before mounting overnight with Permount
345 (Fisher Scientific). Brightfield microscopy on mid-distal histological sections was performed
346 using a 100X objective on an EVOS XL Cell Imaging System (ThermoFisher Scientific) in which

347 5 mid-distal colon sections per mouse per group were blindly assessed using a validated 12-point
348 scoring system[45].

349 **Metabolomics and Transcriptomics** As shown in **Fig. 2a**, matched BMDCs prepared and treated
350 with HnpM for 4 and 20 h were used for metabolomics and transcriptomics. For metabolomics,
351 supernatants and cell-free media controls were collected and incubated with ice-cold HPLC-grade
352 methanol for 30 min on ice, centrifuged at 10,000 × *g* for 10 min at 4°C, and stored at -80°C until
353 analysis. For transcriptomics, RNA from HnpM-treated and control BMDCs was extracted with
354 TRIzol (Life Technologies) and chloroform and precipitated with isopropanol and extracted using
355 PureLink RNA Micro Scale Kit (ThermoFisher).

356 **Metabolomic profiling** The profiling of nonpolar metabolites was performed at the UVic-Genome
357 BC Proteomics Centre by LC-MS/MS analysis of the deproteinated conditioned media by injecting
358 3 mL of sample onto a Dionex UHPLC system equipped with an Agilent Eclipse C_{18} (2.1 × 15
359 mm, 1.8 mm) column incubated at 45°C. Metabolites were resolved with a 30 min linear running
360 0-80% using the buffer system 0.05% formic acid and 0.05% formic acid in acetonitrile at a flow
361 rate of 300 mL/min. The column effluent was introduced by electrospray ionization onto a Velos
362 LTQ Orbitrap Analyzer (Thermo Scientific) using a spray voltage of 3.6 kV, a source heater
363 temperature of 350°C, and a sheath gas flow of 40 l/min. Survey scans were performed using the
364 Orbitrap mass spectrometer and the 10 most intense ions were selected for fragmentation using a
365 30-40 V-stepped collision-induced dissociation energy. Fragmentation products were analyzed in
366 the linear ion trap mass spectrometer. Fragmentation was used to perform an online search using
367 the XCMS database (https://xcmsonline.scripps.edu) to identify possible metabolites.

368 Following peak profiling, 2-fold change enriched peaks (compared to control samples, i.e.,
369 samples with media only) were selected to perform statistical and functional interpretation using

370 MetaboAnalyst 5.0 (https://www.metaboanalyst.ca/)[46]. Data were analyzed using interquartile
371 range (IQR) and normalized by doing a $\log_{10}$ transformation. Principal component (PC) analysis,
372 volcano plot (2-fold change threshold, 0.1 p-value threshold, and equal group variance), and
373 heatmap (with Euclidean distance measure and Ward clustering algorithm with clustered group
374 samples) were performed. Peak annotations were further analyzed using Mummichog algorithm
375 and KEGG database for functional interpretation.

376 **RNA sequencing**

377 RNA sequencing of poly-A enriched RNAs was performed at Centre d'expertise et de services
378 Génome Québec, as previously described[47]. Briefly, libraries were sequenced by Illumina RNA-
379 Seq Libraries on two experimental replicates for each experiment. Reads alignment and gene ID
380 mapping were performed using Bowtie2 and HTSeq, respectively, against the Genome Reference
381 Consortium Mouse Build 38 patch release 6 (GRCm38.p6) database. Read counts were obtained
382 with featureCounts from package subread and differential gene expression was obtained using
383 EdgeR with a quasi-likelihood negative binomial generalized log-linear model likelihood ratio test.
384 One count per million (CPM) minimum per gene, or five counts per gene in the smallest library,
385 and counts represented by at least two replicate libraries were required for a gene to be considered
386 for analysis. Genes were considered differentially expressed if the fold changes were ≥ 2 and $p \leq$
387 0.05. Further GSEA tests were performed using the fgsea and gage packages in R. Gene sets were
388 constructed with genes differentially expressed up and down. Gene sets were analyzed using
389 published data on tolerogenic and inflammatory DCs **(Supp. File)**[39, 48, 49]. Gene sets are
390 represented as a barcode plot using the Limma package in R.

391 **Statistical analysis** Statistical analyses of metabolomic and transcriptomic data are described in
392 each corresponding method sections. All other data are presented as boxplots indicating the median

393 (center line), upper and lower box bounds (IQR = first and third quartiles), and whiskers (minimum
394 and maximum values), with individual data points superimposed onto the boxplot. Normality of
395 datasets were tested using the Kolmogorov-Smirnoff test. Data that were normally distributed were
396 analyzed by one-way ANOVA with appropriate post-hoc tests. Unpaired data were compared
397 using two-tailed unpaired Student's *t* test. Statistical analysis was performed using GraphPad
398 Prism v.9.3.1, and significance was assumed for $p < 0.05$.

399 **FIGURE LEGENDS**

400 **Figure 1. Helminth-derived nonpolar metabolites (HnpM) induce a tolerogenic phenotype in**
401 **DCs**

402 **(a)** Experimental design workflow. Created in BioRender.

403 **(b)** TNF and IL-10 secreted protein quantified by ELISA from BMDCs either untreated controls
404 or treated with 50 μg/ml helminth-derived polar metabolites (HpM), 50 μg/ml HnpM, or 50
405 μg/ml of mock-extracted polar/nonpolar media controls for 20 h, and then stimulated with 100
406 ng/ml LPS for 4 h. Data are represented as boxplots and analyzed by one-way ANOVA with
407 Holm-Sidak multiple comparisons: ****$p<0.0001$, ***$p<0.001$, n=4 biological replicates for
408 BMDCs from 4 individual mice per group.

409 **(c)** Ratio of secreted TNF/IL-10 based on data presented in Figure 1a. Data are represented as
410 boxplots and analyzed by unpaired t test: $p=0.0022$, n=4 individual mice per group.

411 **(d)** Gating strategy used to assess CD45/CD11c$^+$ BMDC populations.

412 **(e)** FACS analysis of MHC-II, CD86, and CD40 expression assessed by BMDCs were treated
413 with vehicle control (PBS) or 50 μg/ml HnpM for 20 h. Data are represented as boxplots and
414 analyzed by unpaired t test: $p=0.0447$, $p=0.0391$, $p=0.0007$, for MHC-II, CD86 and CD40,
415 respectively. n=4 biological replicates for BMDCs from 4 individual mice/group that were
416 isolated, differentiated, and treated as described.

417 **(f)** Gating strategy used to assess splenic CD45/CD11c$^+$ DC populations.

418 **(g)** Splenic DC surface expression of MHC-II, CD86, and CD40 assessed by flow cytometry. Mice
419 were injected i.p. with 25 μg HnpM or PBS as a control per day for 3 days and splenic DCs
420 were isolated for flow cytometry. Data are represented as boxplots and analyzed by unpaired t
421 test: $p=0.0260$, $p=0.0194$, $p=0.0066$, for MHC-II, CD86 and CD40, respectively. n=biological
422 replicates of splenic DCs from 5 individual mice per group.

423 **(h)** Gating strategy used to assess the proliferation of CD4$^+$CD44$^+$ T cells co-cultured with either
424 control (PBS) or HnpM-treated BMDCs for 72 h. Plots indicate the CFSE$^+$ cells in gated
425 CD4$^+$CD44$^+$T cells.

426 **(i)** Data presented as mean fluorescence intensity of CSFE dye dilution in gated CD4$^+$CD44$^+$ T
427 cells and the percentage of cells undergoing > 3 cell divisions.

428 **(j)** Histogram of the percentage of CD4$^+$CD44$^+$ T cells undergoing > 3 cell divisions. Data are
429 represented as bar graphs with experimental replicate data points and analyzed by paired *t* test:

430 p=0.0001 (top), p=0.0429 (bottom). n=3 biological replicates for $CD4^+CD44^+$ T cells obtained
431 from 3 individual OT-II mice.
432 **(k)** Gating strategy used to assess $Foxp3^+$ populations in gated $CD4^+$ T cells co-cultured with
433 control or HnpM-treated BMDCs.
434 **(l)** $CD4^+$ T cell expression of Foxp3 assessed by flow cytometry. BMDCs were treated with either
435 vehicle control (PBS) or 50 μg/ml HnpM for 20 h, and co-cultured for 48 h with OT-II $CD4^+$
436 T cells isolated from spleen by negative selection using magnetic beads. Data are represented
437 as boxplots and analyzed by unpaired t test: p= 0.0077, n=6 biological replicates of BMDCs
438 from 4 individual mice per group.
439
440 **Figure 2. Helminth-derived nonpolar metabolites (HnpM) induce metabolic changes in**
441 **BMDCs.**
442 **(a)** Experimental design workflow schematic of matched metabolomics and transcriptomics
443 experiments. BMDCs were isolated and differentiated with 20 ng/ml GM-CSF and treated with
444 HnpM or vehicle control (PBS) for 4 and 20 h. The supernatants were collected for untargeted
445 metabolomics analysis and mRNA was extracted for RNA sequencing. n=biological replicates
446 from 3 individual mice per group of BMDCs. Graphic created in BioRender.
447 **(b)** Heatmap of top 50 statistically enriched peak intensities at 4 h. Hierarchical clustering of
448 metabolite concentrations with a higher enrichment (red) and lower enrichment (blue) were
449 determined by Euclidean distance measuring and Ward clustering algorithms.
450 **(c)** Principal component (PC) analysis was performed using the prcomp package. The calculation
451 was based on singular value decomposition and the Rscript chemometrics. The 2-D score plots
452 between selected PCs are shown and the respective variances are provided.
453 **(d)** Scatter plot of inferred pathways with potential matched compounds. The peak annotations
454 were performed using the Mummichog algorithm and the KEGG database was used for
455 functional interpretation.
456
457 **Figure 3. Helminth-derived nonpolar metabolites (HnpM) induce a unique transcriptomic**
458 **signature in BMDCs.**
459 Data for BMDCs treated with HnpM or vehicle control (PBS) for 20 h are presented. RNA was
460 extracted as described in Materials and Methods for RNA sequencing by Illumina RNA-seq. Reads

461 alignment and gene ID mapping were performed using Bowtie2 and HTSeq, respectively, against
462 the Genome Reference Consortium Mouse Build 38 patch release 6 (GRCm38.p6) database.
463 **(a)** Venn diagram and **(b)** volcano plot for differentially expressed genes at 20 h. Read counts
464 were obtained with Get_ReadCount.py and differential gene expression was obtained using
465 EdgeR with a likelihood ratio test. Genes were considered differentially expressed if the fold
466 change ≥ 2 and $p \leq 0.05$.
467 **(c)** GO annotation and pathway enrichment. All statistically enriched terms were identified based
468 on the default choices under accumulative hypergeometric p-values and enrichment factors
469 were calculated and used for filtering. Remaining significant terms were then hierarchically
470 clustered into a tree based on Kappa-statistical similarities among their gene memberships.
471 Then 0.3 kappa score was applied as the threshold to cast the tree into term clusters.
472 **(d)** Protein-protein interaction (PPI) network among the input genes. A subset of representative
473 terms from the full cluster was converted into a network layout and each term is represented
474 by a circular node, where the size is proportional to the number of input genes falling under
475 that term with similar color representing cluster identity. Terms with a similarity score > 0.3
476 are linked by an edge and the thickness of the edge represents the similarity score.
477 **(e)** GSEA analysis was performed with phenoTest package in R. Gene sets were constructed with
478 genes that are differentially expressed up and down. Gene sets were analyzed using published
479 data on tolerogenic and inflammatory DCs **(Supp. File)** Gene sets are represented using a
480 barcode plot using the Limma package in R.
481 **(f)** Integrative analysis of transcriptional and metabolic signatures. Enrichment analysis by
482 hypergeometric test and topology measured degree centrality. Combined queries integration
483 method was performed, and the overviews indicate all matched pathways according to the p
484 values from the pathway enrichment analysis and pathway impact values from the pathway
485 topology analysis.
486
487 **Figure 4. DCs treated with HnpM alleviate DSS-induced intestinal inflammation.**
488 Intestinal inflammation was chemically-induced in B6 mice by administration of 3% DSS in
489 drinking water for 5 days. On day 5, mice were injected i.p. with PBS as a control or 1 x 10^6 naïve
490 BMDCs or HnpM-treated BMDCs. Mice without DSS served as a negative control. Control mice

491 and mice adoptively transferred with BMDCs were sacrificed on day 8 post-DSS and necropsies
492 were performed to determine the following:
493 **(a)** Disease activity scores (DAS) on a scale from 0-5 were determined based on body weight,
494 colon length, health of the animal, rectal bleeding, and macroscopic appearance of the colon.
495 **(b)** Colon lengths in cm.
496 **(c)** Percent weight changes were determined on day 8 as a percentage compared to weight before
497 DSS exposure.
498 **(d)** Histopathology scores (left) assessed in 5 sections per mouse per group of H&E-stained mid-
499 distal colon sections (right).
500 Data in **Fig. 4a-d** are represented as boxplots and analyzed by one-way ANOVA with Holm-Sidak
501 multiple comparisons: ****$p<0.0001$, ***$p<0.001$, n=4-5 mice per group.
502
503 **COMPETING INTERESTS**
504 The authors declare no competing interests.
505
506 **DATA AVAILABILITY**
507 Source data associated with Figure and Supplemental Figure panels are provided with this paper
508 as a Source Data file. Metabolite LC-MS data was deposited to Metabolomics Workbench under
509 accession number ST002230. Transcriptomics data (RNAseq) was deposited to the NCBI
510 Sequence Read Archive (SRA) under accession number PRJNA856720.
511

512 **REFERENCES**
513

514 1. Baumgart, D. C. and Sandborn, W. J. (2012) Crohn's disease. Lancet (London, England)
515 380, 1590-605.
516 2. Ordas, I., Eckmann, L., Talamini, M., Baumgart, D. C., Sandborn, W. J. (2012) Ulcerative
517 colitis. Lancet (London, England) 380, 1606-19.
518 3. Luciani, C., Hager, F. T., Cerovic, V., Lelouard, H. (2022) Dendritic cell functions in the
519 inductive and effector sites of intestinal immunity. Mucosal Immunol 15, 40-50.
520 4. Kaplan, G. G. (2014) IBD: Global variations in environmental risk factors for IBD. Nature
521 reviews. Gastroenterology & hepatology 11, 708-9.
522 5. Witowski, J., Pawlaczyk, K., Breborowicz, A., Scheuren, A., Kuzlan-Pawlaczyk, M.,
523 Wisniewska, J., Polubinska, A., Friess, H., Gahl, G. M., Frei, U., Jörres, A. (2000) IL-17
524 stimulates intraperitoneal neutrophil infiltration through the release of GRO alpha
525 chemokine from mesothelial cells. J Immunol 165, 5814-21.
526 6. Maloy, K. J. and Powrie, F. (2011) Intestinal homeostasis and its breakdown in
527 inflammatory bowel disease. Nature 474, 298-306.
528 7. Weaver, C. T., Elson, C. O., Fouser, L. A., Kolls, J. K. (2013) The Th17 pathway and
529 inflammatory diseases of the intestines, lungs, and skin. Annu Rev Pathol 8, 477-512.
530 8. Strober, W. (2006) Immunology. Unraveling gut inflammation. Science 313, 1052-4.
531 9. Fuss, I. J., Heller, F., Boirivant, M., Leon, F., Yoshida, M., Fichtner-Feigl, S., Yang, Z.,
532 Exley, M., Kitani, A., Blumberg, R. S., Mannon, P., Strober, W. (2004) Nonclassical
533 CD1d-restricted NK T cells that produce IL-13 characterize an atypical Th2 response in
534 ulcerative colitis. J Clin Invest 113, 1490-7.
535 10. Heller, F., Fuss, I. J., Nieuwenhuis, E. E., Blumberg, R. S., Strober, W. (2002) Oxazolone
536 colitis, a Th2 colitis model resembling ulcerative colitis, is mediated by IL-13-producing
537 NK-T cells. Immunity 17, 629-38.
538 11. Setiawan, T., Metwali, A., Blum, A. M., Ince, M. N., Urban, J. F., Jr., Elliott, D. E.,
539 Weinstock, J. V. (2007) Heligmosomoides polygyrus promotes regulatory T-cell cytokine
540 production in the murine normal distal intestine. Infect Immun 75, 4655-63.
541 12. Elliott, D. E., Setiawan, T., Metwali, A., Blum, A., Urban, J. F., Jr., Weinstock, J. V. (2004)
542 Heligmosomoides polygyrus inhibits established colitis in IL-10-deficient mice. Eur J
543 Immunol 34, 2690-8.
544 13. Elliott, D. E., Urban, J. J., Argo, C. K., Weinstock, J. V. (2000) Does the failure to acquire
545 helminthic parasites predispose to Crohn's disease? Faseb j 14, 1848-55.
546 14. Khan, W. I., Blennerhasset, P. A., Varghese, A. K., Chowdhury, S. K., Omsted, P., Deng,
547 Y., Collins, S. M. (2002) Intestinal nematode infection ameliorates experimental colitis in
548 mice. Infect Immun 70, 5931-7.
549 15. Hang, L., Blum, A. M., Kumar, S., Urban, J. F., Jr., Mitreva, M., Geary, T. G., Jardim, A.,
550 Stevenson, M. M., Lowell, C. A., Weinstock, J. V. (2016) Downregulation of the Syk
551 Signaling Pathway in Intestinal Dendritic Cells Is Sufficient To Induce Dendritic Cells
552 That Inhibit Colitis. J Immunol 197, 2948-57.
553 16. Arai, T., Lopes, F., Shute, A., Wang, A., McKay, D. M. (2018) Young mice expel the
554 tapeworm Hymenolepis diminuta and are protected from colitis by triggering a memory
555 response with worm antigen. American journal of physiology. Gastrointestinal and liver
556 physiology 314, G461-g470.

17. Wang, A., Arai, T., Campbell, A., Reyes, J. L., Lopes, F., McKay, D. M. (2017) Triggering immunological memory against the tapeworm Hymenolepis diminuta to protect against colitis. Parasite Immunol 39.
18. Elliott, D. E., Li, J., Blum, A., Metwali, A., Qadir, K., Urban, J. F., Jr., Weinstock, J. V. (2003) Exposure to schistosome eggs protects mice from TNBS-induced colitis. American journal of physiology. Gastrointestinal and liver physiology 284, G385-91.
19. Iberg, C. A., Jones, A., Hawiger, D. (2017) Dendritic Cells As Inducers of Peripheral Tolerance. Trends in Immunology 38, 793-804.
20. Vendelova, E., Ashour, D., Blank, P., Erhard, F., Saliba, A. E., Kalinke, U., Lutz, M. B. (2018) Tolerogenic Transcriptional Signatures of Steady-State and Pathogen-Induced Dendritic Cells. Front Immunol 9, 333.
21. Adalid-Peralta, L., Arce-Sillas, A., Fragoso, G., Cárdenas, G., Rosetti, M., Casanova-Hernández, D., Rangel-Escareño, C., Uribe-Figueroa, L., Fleury, A., Sciutto, E. (2013) Cysticerci drive dendritic cells to promote in vitro and in vivo Tregs differentiation. Clin Dev Immunol 2013, 981468.
22. Yap, G. S. and Gause, W. C. (2018) Helminth Infections Induce Tissue Tolerance Mitigating Immunopathology but Enhancing Microbial Pathogen Susceptibility. Frontiers in Immunology 9.
23. Segura, M., Su, Z., Piccirillo, C., Stevenson, M. M. (2007) Impairment of dendritic cell function by excretory-secretory products: A potential mechanism for nematode-induced immunosuppression. European Journal of Immunology 37, 1887-1904.
24. Gause, W. C., Urban, J. F., Jr., Stadecker, M. J. (2003) The immune response to parasitic helminths: insights from murine models. Trends Immunol 24, 269-77.
25. Thomas, P. G. and Harn, D. A., Jr. (2004) Immune biasing by helminth glycans. Cell Microbiol 6, 13-22.
26. Balic, A., Harcus, Y., Holland, M. J., Maizels, R. M. (2004) Selective maturation of dendritic cells by Nippostrongylus brasiliensis-secreted proteins drives Th2 immune responses. Eur J Immunol 34, 3047-59.
27. Whelan, M., Harnett, M. M., Houston, K. M., Patel, V., Harnett, W., Rigley, K. P. (2000) A filarial nematode-secreted product signals dendritic cells to acquire a phenotype that drives development of Th2 cells. J Immunol 164, 6453-60.
28. Cronin, J. G., Kanamarlapudi, V., Thornton, C. A., Sheldon, I. M. (2016) Signal transducer and activator of transcription-3 licenses Toll-like receptor 4-dependent interleukin (IL)-6 and IL-8 production via IL-6 receptor-positive feedback in endometrial cells. Mucosal Immunol 9, 1125-36.
29. Kane, C. M., Cervi, L., Sun, J., McKee, A. S., Masek, K. S., Shapira, S., Hunter, C. A., Pearce, E. J. (2004) Helminth Antigens Modulate TLR-Initiated Dendritic Cell Activation. The Journal of Immunology 173, 7454.
30. Matteoli, G., Mazzini, E., Iliev, I. D., Mileti, E., Fallarino, F., Puccetti, P., Chieppa, M., Rescigno, M. (2010) Gut CD103⁺ dendritic cells express indoleamine 2,3-dioxygenase which influences T regulatory/T effector cell balance and oral tolerance induction. Gut 59, 595.
31. Muralidharan, S., Torta, F., Lin, M. K., Olona, A., Bagnati, M., Moreno-Moral, A., Ko, J. H., Ji, S., Burla, B., Wenk, M. R., Rodrigues, H. G., Petretto, E., Behmoaras, J. (2022) Immunolipidomics Reveals a Globoside Network During the Resolution of Pro-Inflammatory Response in Human Macrophages. Front Immunol 13, 926220.

603 32. Mohammed, S., Vineetha, N. S., James, S., Aparna, J. S., Babu Lankadasari, M., Maeda,
604 T., Ghosh, A., Saha, S., Li, Q. Z., Spiegel, S., Harikumar, K. B. (2020) Regulatory role of
605 SphK1 in TLR7/9-dependent type I interferon response and autoimmunity. Faseb j 34,
606 4329-4347.
607 33. Sun, D. and Fernandes, G. (2003) Lovastatin inhibits bone marrow-derived dendritic cell
608 maturation and upregulates proinflammatory cytokine production. Cell Immunol 223, 52-
609 62.
610 34. Nikolic, T., Woittiez, N. J. C., van der Slik, A., Laban, S., Joosten, A., Gysemans, C.,
611 Mathieu, C., Zwaginga, J. J., Koeleman, B., Roep, B. O. (2017) Differential transcriptome
612 of tolerogenic versus inflammatory dendritic cells points to modulated T1D genetic risk
613 and enriched immune regulation. Genes Immun 18, 176-183.
614 35. Navarro-Barriuso, J., Mansilla, M. J., Naranjo-Gómez, M., Sánchez-Pla, A., Quirant-
615 Sánchez, B., Teniente-Serra, A., Ramo-Tello, C., Martínez-Cáceres, E. M. (2018)
616 Comparative transcriptomic profile of tolerogenic dendritic cells differentiated with
617 vitamin D3, dexamethasone and rapamycin. Scientific Reports 8, 14985.
618 36. Li, X., Egervari, G., Wang, Y., Berger, S. L., Lu, Z. (2018) Regulation of chromatin and
619 gene expression by metabolic enzymes and metabolites. Nature Reviews Molecular Cell
620 Biology 19, 563-578.
621 37. Harry, R. A., Anderson, A. E., Isaacs, J. D., Hilkens, C. M. (2010) Generation and
622 characterisation of therapeutic tolerogenic dendritic cells for rheumatoid arthritis. Ann
623 Rheum Dis 69, 2042-50.
624 38. Széles, L., Keresztes, G., Töröcsik, D., Balajthy, Z., Krenács, L., Póliska, S., Steinmeyer,
625 A., Zuegel, U., Pruenster, M., Rot, A., Nagy, L. (2009) 1,25-dihydroxyvitamin D3 is an
626 autonomous regulator of the transcriptional changes leading to a tolerogenic dendritic cell
627 phenotype. J Immunol 182, 2074-83.
628 39. Shao, S., Cui, D., Ma, C., Chen, P., Zhou, B., Tao, R., Wang, J. (2020) Transcriptome
629 profiling of tolerogenic dendritic cells conditioned with dual mTOR kinase inhibitor,
630 AZD8055. Int Immunopharmacol 81, 106241.
631 40. Reed, M., Luissint, A. C., Azcutia, V., Fan, S., O'Leary, M. N., Quiros, M., Brazil, J.,
632 Nusrat, A., Parkos, C. A. (2019) Epithelial CD47 is critical for mucosal repair in the murine
633 intestine in vivo. Nat Commun 10, 5004.
634 41. Matisz, C. E., Geuking, M. B., Lopes, F., Petri, B., Wang, A., Sharkey, K. A., McKay, D.
635 M. (2018) Helminth Antigen-Conditioned Dendritic Cells Generate Anti-Inflammatory
636 Cd4 T Cells Independent of Antigen Presentation via Major Histocompatibility Complex
637 Class II. Am J Pathol 188, 2589-2604.
638 42. Reyes, J. L., Lopes, F., Leung, G., Jayme, T. S., Matisz, C. E., Shute, A., Burkhard, R.,
639 Carneiro, M., Workentine, M. L., Wang, A., Petri, B., Beck, P. L., Geuking, M. B., McKay,
640 D. M. (2019) Macrophages treated with antigen from the tapeworm Hymenolepis diminuta
641 condition CD25(+) T cells to suppress colitis. Faseb j 33, 5676-5689.
642 43. Matisz, C. E., Leung, G., Reyes, J. L., Wang, A., Sharkey, K. A., McKay, D. M. (2015)
643 Adoptive transfer of helminth antigen-pulsed dendritic cells protects against the
644 development of experimental colitis in mice. Eur J Immunol 45, 3126-39.
645 44. Valanparambil, R. M., Segura, M., Tam, M., Jardim, A., Geary, T. G., Stevenson, M. M.
646 (2014) Production and analysis of immunomodulatory excretory-secretory products from
647 the mouse gastrointestinal nematode Heligmosomoides polygyrus bakeri. Nat Protoc 9,
648 2740-54.

649 45. Lopes, F., Wang, A., Smyth, D., Reyes, J. L., Doering, A., Schenck, L. P., Beck, P.,
650 Waterhouse, C., McKay, D. M. (2015) The Src kinase Fyn is protective in acute chemical-
651 induced colitis and promotes recovery from disease. J Leukoc Biol 97, 1089-99.
652 46. Pang, Z., Zhou, G., Ewald, J., Chang, L., Hacariz, O., Basu, N., Xia, J. (2022) Using
653 MetaboAnalyst 5.0 for LC-HRMS spectra processing, multi-omics integration and
654 covariate adjustment of global metabolomics data. Nat Protoc.
655 47. Rodríguez-García, A., Sola-Landa, A., Pérez-Redondo, R. (2021) Coupled
656 Transcriptomics for Differential Expression Analysis and Determination of Transcription
657 Start Sites: Design and Bioinformatics. Methods Mol Biol 2296, 263-278.
658 48. Lee, E. G., Jung, N. C., Lee, J. H., Song, J. Y., Ryu, S. Y., Seo, H. G., Han, S. G., Ahn, K.
659 J., Hong, K. S., Choi, J., Lim, D. S. (2016) Tolerogenic dendritic cells show gene
660 expression profiles that are different from those of immunogenic dendritic cells in DBA/1
661 mice. Autoimmunity 49, 90-101.
662 49. Chen, Z., Gordon, J. R., Zhang, X., Xiang, J. (2002) Analysis of the gene expression
663 profiles of immature versus mature bone marrow-derived dendritic cells using DNA arrays.
664 Biochem Biophys Res Commun 290, 66-72.
665

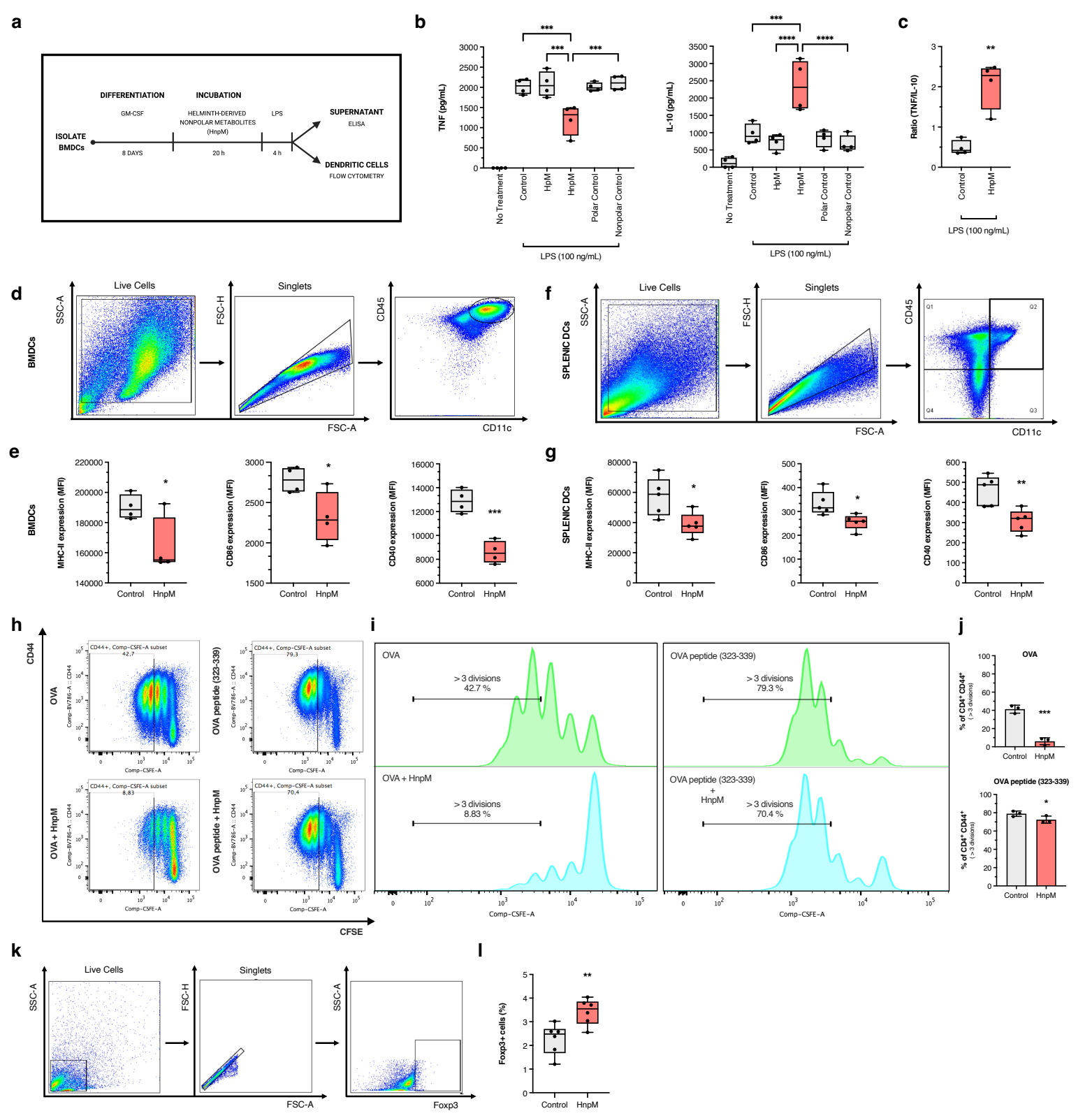
a
DIFFERENTIATION
INCUBATION
GM-CSF
HELMINTH-DERIVED NONPOLAR METABOLITES (HnpM)
LPS
SUPERNATANT
ELISA
ISOLATE BMDCs
8 DAYS
20 h
4 h
DENDRITIC CELLS
FLOW CYTOMETRY
b
TNF (pg/mL)
IL-10 (pg/mL)
No Treatment
Control
HpM
HnpM
Polar Control
Nonpolar Control
LPS (100 ng/mL)
c
Ratio (TNF/IL-10)
Control
HnpM
LPS (100 ng/mL)
d
BMDCs
Live Cells
Singlets
SSC-A
FSC-H
FSC-A
CD45
CD11c
f
SPLENIC DCs
Live Cells
Singlets
SSC-A
FSC-H
FSC-A
CD45
CD11c
e
BMDCs
MHC-II expression (MFI)
CD86 expression (MFI)
CD40 expression (MFI)
Control
HnpM
g
SPLENIC DCs
MHC-II expression (MFI)
CD86 expression (MFI)
CD40 expression (MFI)
Control
HnpM
h
CD44
CFSE
OVA
OVA peptide (323-339)
OVA + HnpM
OVA peptide + HnpM
Comp-CSFE-A
i
OVA
> 3 divisions
42.7 %
OVA peptide (323-339)
> 3 divisions
79.3 %
OVA + HnpM
> 3 divisions
8.83 %
OVA peptide (323-339) + HnpM
> 3 divisions
70.4 %
Comp-CSFE-A
j
OVA
OVA peptide (323-339)
% of CD4+ CD44+ (> 3 divisions)
Control
HnpM
k
Live Cells
Singlets
SSC-A
FSC-H
FSC-A
Foxp3
l
Foxp3+ cells (%)
Control
HnpM

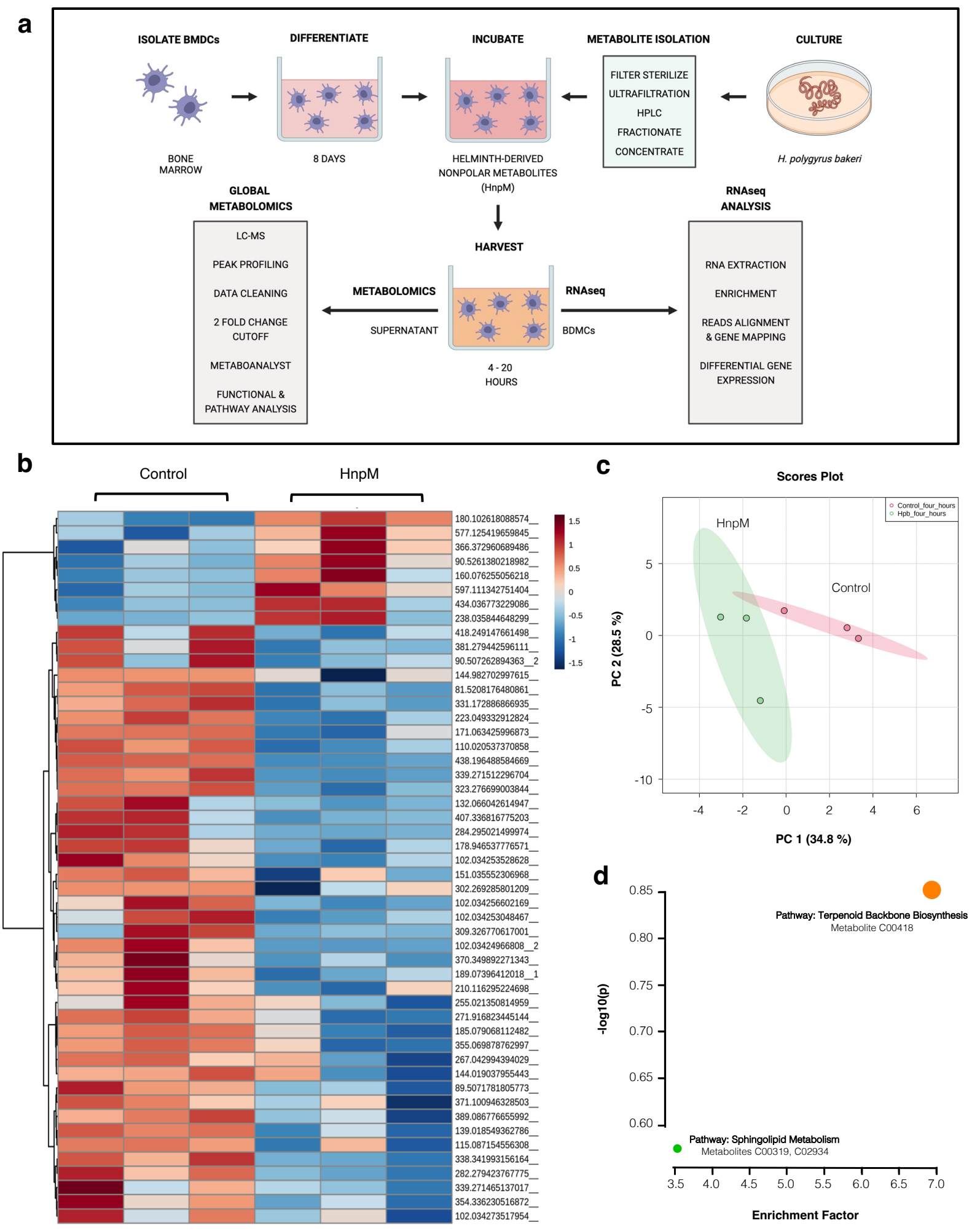
a
ISOLATE BMDCs
DIFFERENTIATE
INCUBATE
METABOLITE ISOLATION
CULTURE
BONE MARROW
8 DAYS
HELMINTH-DERIVED NONPOLAR METABOLITES (HnpM)
FILTER STERILIZE
ULTRAFILTRATION
HPLC
FRACTIONATE
CONCENTRATE
H. polygyrus bakeri
GLOBAL METABOLOMICS
LC-MS
PEAK PROFILING
DATA CLEANING
2 FOLD CHANGE CUTOFF
METABOANALYST
FUNCTIONAL & PATHWAY ANALYSIS
HARVEST
METABOLOMICS
SUPERNATANT
RNAseq
BDMCs
4 - 20 HOURS
RNAseq ANALYSIS
RNA EXTRACTION
ENRICHMENT
READS ALIGNMENT & GENE MAPPING
DIFFERENTIAL GENE EXPRESSION
b
Control
HnpM
180.102618088574__
577.125419659845__
366.372960689486__
90.5261380218982__
160.076255056218__
597.111342751404__
434.036773229086__
238.035844648299__
418.249147661498__
381.279442596111__
90.507262894363__2
144.982702997615__
81.5208176480861__
331.172886866935__
223.049332912824__
171.063425996873__
110.020537370858__
438.196488584669__
339.271512296704__
323.276699003844__
132.066042614947__
407.336816775203__
284.295021499974__
178.946537776571__
102.034253528628__
151.035552306968__
302.269285801209__
102.034256602169__
102.034253048467__
309.326770617001__
102.03424966808__2
370.349892271343__
189.07396412018__1
210.116295224698__
255.021350814959__
271.916823445144__
185.079068112482__
355.069878762997__
267.042994394029__
144.019037955443__
89.5071781805773__
371.100946328503__
389.086776655992__
139.018549362786__
115.087154556308__
338.341993156164__
282.279423767775__
339.271465137017__
354.336230516872__
102.034273517954__
1.5
1
0.5
0
-0.5
-1
-1.5
c
Scores Plot
Control_four_hours
Hpb_four_hours
HnpM
Control
PC 2 (28.5 %)
PC 1 (34.8 %)
5
0
-5
-10
-4
-2
0
2
4
6
d
-log10(p)
0.85
0.80
0.75
0.70
0.65
0.60
Pathway: Terpenoid Backbone Biosynthesis
Metabolite C00418
Pathway: Sphingolipid Metabolism
Metabolites C00319, C02934
3.5
4.0
4.5
5.0
5.5
6.0
6.5
7.0
Enrichment Factor

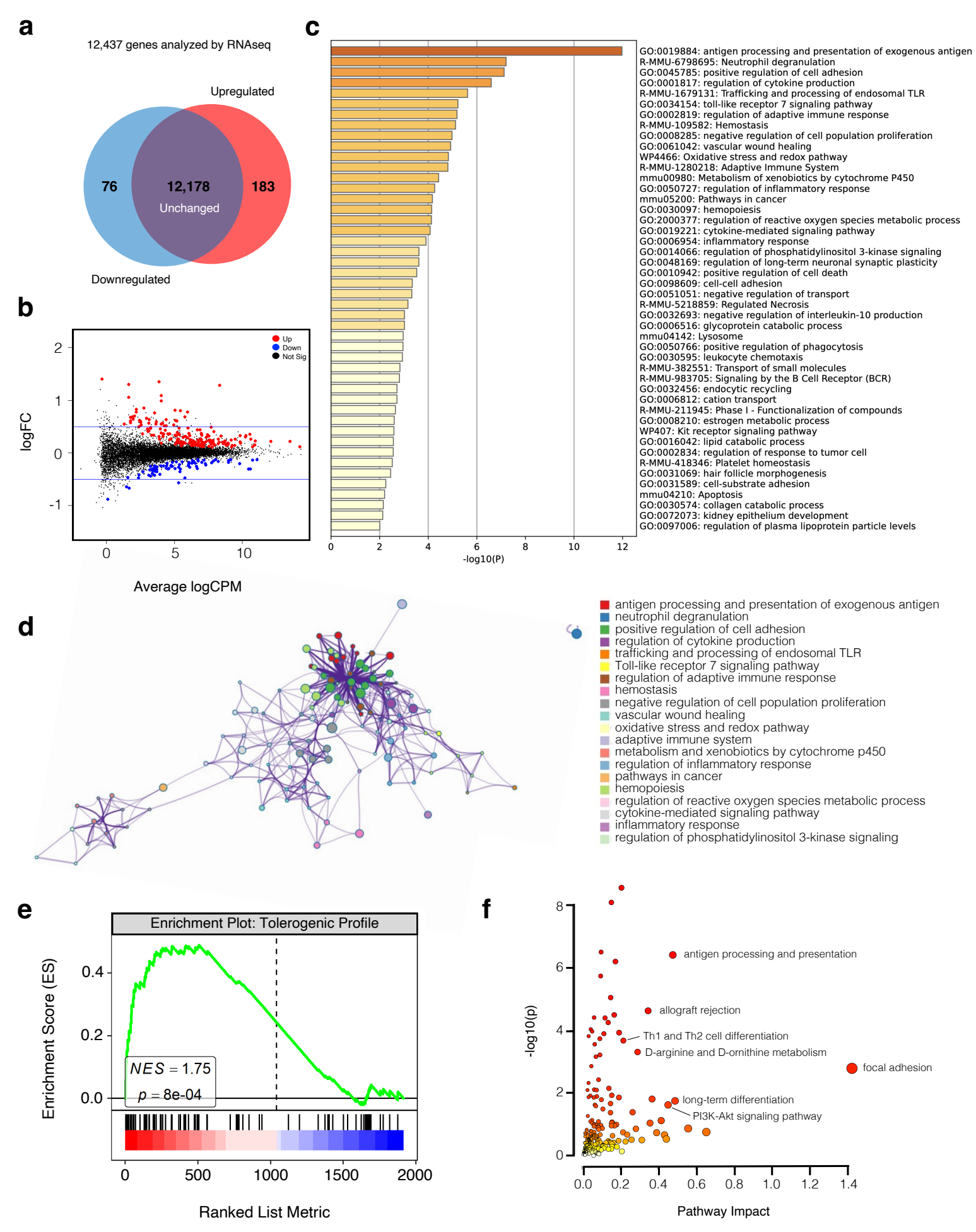
a
12,437 genes analyzed by RNAseq
Upregulated
76
12,178
183
Unchanged
Downregulated
b
Up
Down
Not Sig
logFC
Average logCPM
c
GO:0019884: antigen processing and presentation of exogenous antigen
R-MMU-6798695: Neutrophil degranulation
GO:0045785: positive regulation of cell adhesion
GO:0001817: regulation of cytokine production
R-MMU-1679131: Trafficking and processing of endosomal TLR
GO:0034154: toll-like receptor 7 signaling pathway
GO:0002819: regulation of adaptive immune response
R-MMU-109582: Hemostasis
GO:0008285: negative regulation of cell population proliferation
GO:0061042: vascular wound healing
WP4466: Oxidative stress and redox pathway
R-MMU-1280218: Adaptive Immune System
mmu00980: Metabolism of xenobiotics by cytochrome P450
GO:0050727: regulation of inflammatory response
mmu05200: Pathways in cancer
GO:0030097: hemopoiesis
GO:2000377: regulation of reactive oxygen species metabolic process
GO:0019221: cytokine-mediated signaling pathway
GO:0006954: inflammatory response
GO:0014066: regulation of phosphatidylinositol 3-kinase signaling
GO:0048169: regulation of long-term neuronal synaptic plasticity
GO:0010942: positive regulation of cell death
GO:0098609: cell-cell adhesion
GO:0051051: negative regulation of transport
R-MMU-5218859: Regulated Necrosis
GO:0032693: negative regulation of interleukin-10 production
GO:0006516: glycoprotein catabolic process
mmu04142: Lysosome
GO:0050766: positive regulation of phagocytosis
GO:0030595: leukocyte chemotaxis
R-MMU-382551: Transport of small molecules
R-MMU-983705: Signaling by the B Cell Receptor (BCR)
GO:0032456: endocytic recycling
GO:0006812: cation transport
R-MMU-211945: Phase I - Functionalization of compounds
GO:0008210: estrogen metabolic process
WP407: Kit receptor signaling pathway
GO:0016042: lipid catabolic process
GO:0002834: regulation of response to tumor cell
R-MMU-418346: Platelet homeostasis
GO:0031069: hair follicle morphogenesis
GO:0031589: cell-substrate adhesion
mmu04210: Apoptosis
GO:0030574: collagen catabolic process
GO:0072073: kidney epithelium development
GO:0097006: regulation of plasma lipoprotein particle levels
-log10(P)
d
antigen processing and presentation of exogenous antigen
neutrophil degranulation
positive regulation of cell adhesion
regulation of cytokine production
trafficking and processing of endosomal TLR
Toll-like receptor 7 signaling pathway
regulation of adaptive immune response
hemostasis
negative regulation of cell population proliferation
vascular wound healing
oxidative stress and redox pathway
adaptive immune system
metabolism and xenobiotics by cytochrome p450
regulation of inflammatory response
pathways in cancer
hemopoiesis
regulation of reactive oxygen species metabolic process
cytokine-mediated signaling pathway
inflammatory response
regulation of phosphatidylinositol 3-kinase signaling
e
Enrichment Plot: Tolerogenic Profile
Enrichment Score (ES)
NES = 1.75
p = 8e-04
Ranked List Metric
f
antigen processing and presentation
allograft rejection
Th1 and Th2 cell differentiation
D-arginine and D-ornithine metabolism
focal adhesion
long-term differentiation
PI3K-Akt signaling pathway
-log10(p)
Pathway Impact

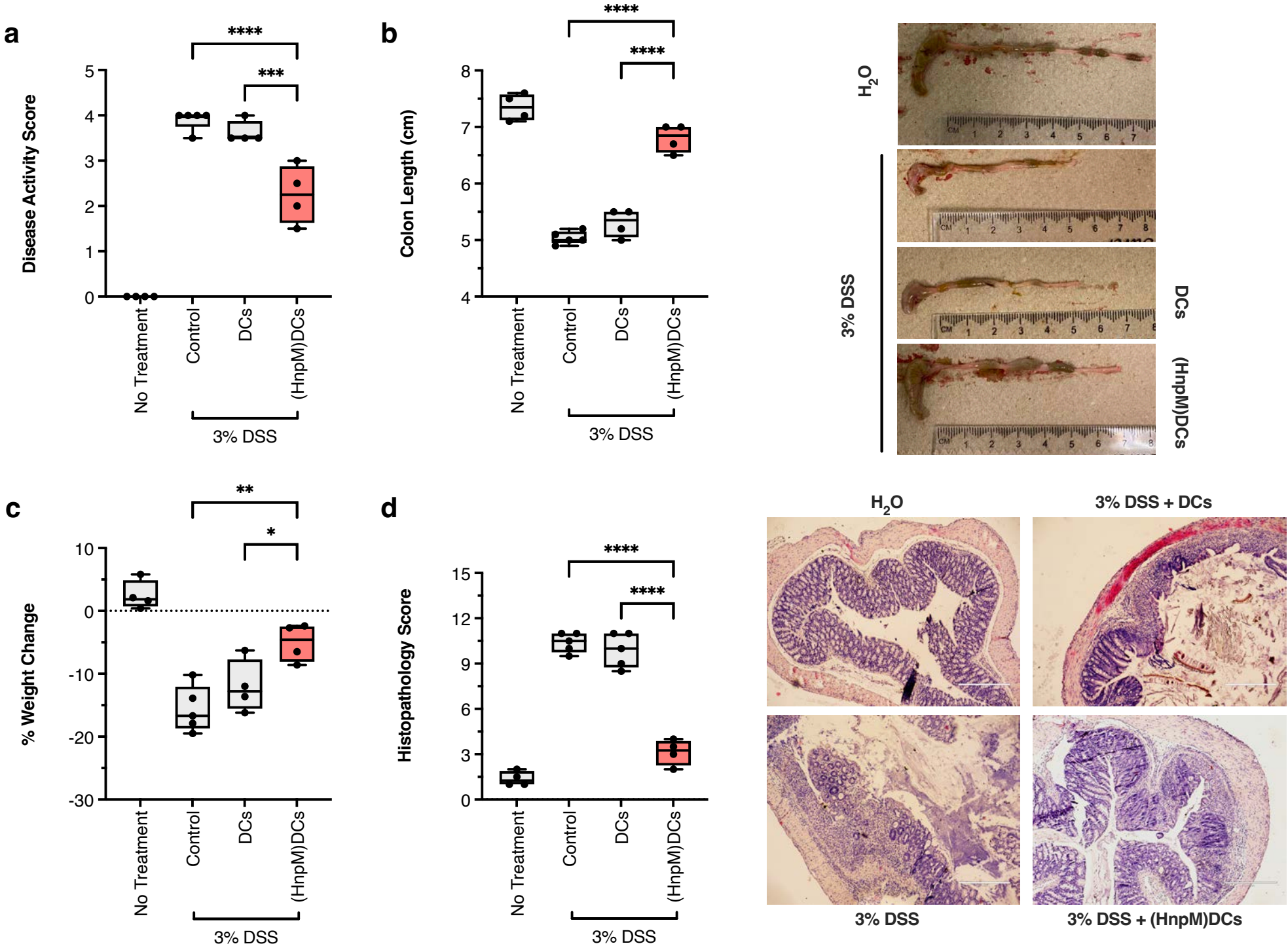
a
Disease Activity Score
****
***
No Treatment
Control
DCs
(HnpM)DCs
3% DSS
b
Colon Length (cm)
****
****
No Treatment
Control
DCs
(HnpM)DCs
3% DSS
H2O
3% DSS
DCs
(HnpM)DCs
c
% Weight Change
**
*
No Treatment
Control
DCs
(HnpM)DCs
3% DSS
d
Histopathology Score
****
****
No Treatment
Control
DCs
(HnpM)DCs
3% DSS
H2O
3% DSS + DCs
3% DSS
3% DSS + (HnpM)DCs

Supplementary Information

Helminth-derived metabolites induce tolerogenic transcriptional and metabolic signatures in dendritic cells in experimental intestinal inflammation

Nathalia L. Malacco[1]*, Aubrey N. Michi[2,3]*, Elizabeth Siciliani[1], Ana G. Madrigal[1], Tamara Sternlieb[1], Ghislaine Fontes[4], Irah L. King[4], Igor Cestari[1], Armando Jardim[1], Mary M. Stevenson[1,4], Fernando Lopes[1,4]

[1]Institute of Parasitology, McGill University, Ste-Anne-de-Bellevue, QC, H9X 3V9, Canada

[2]Department of Cancer Biology, Dana-Farber Cancer Institute, Boston, MA, 02215, USA

[3]Department of Cell Biology, Harvard Medical School, Boston, MA, 02215, USA

[4]Department of Microbiology and Immunology, McGill University, Montreal, QC, H3A 2B4

*Equal contribution

Correspondence: fernando.lopes@mcgill.ca

Supplementary Figure 1

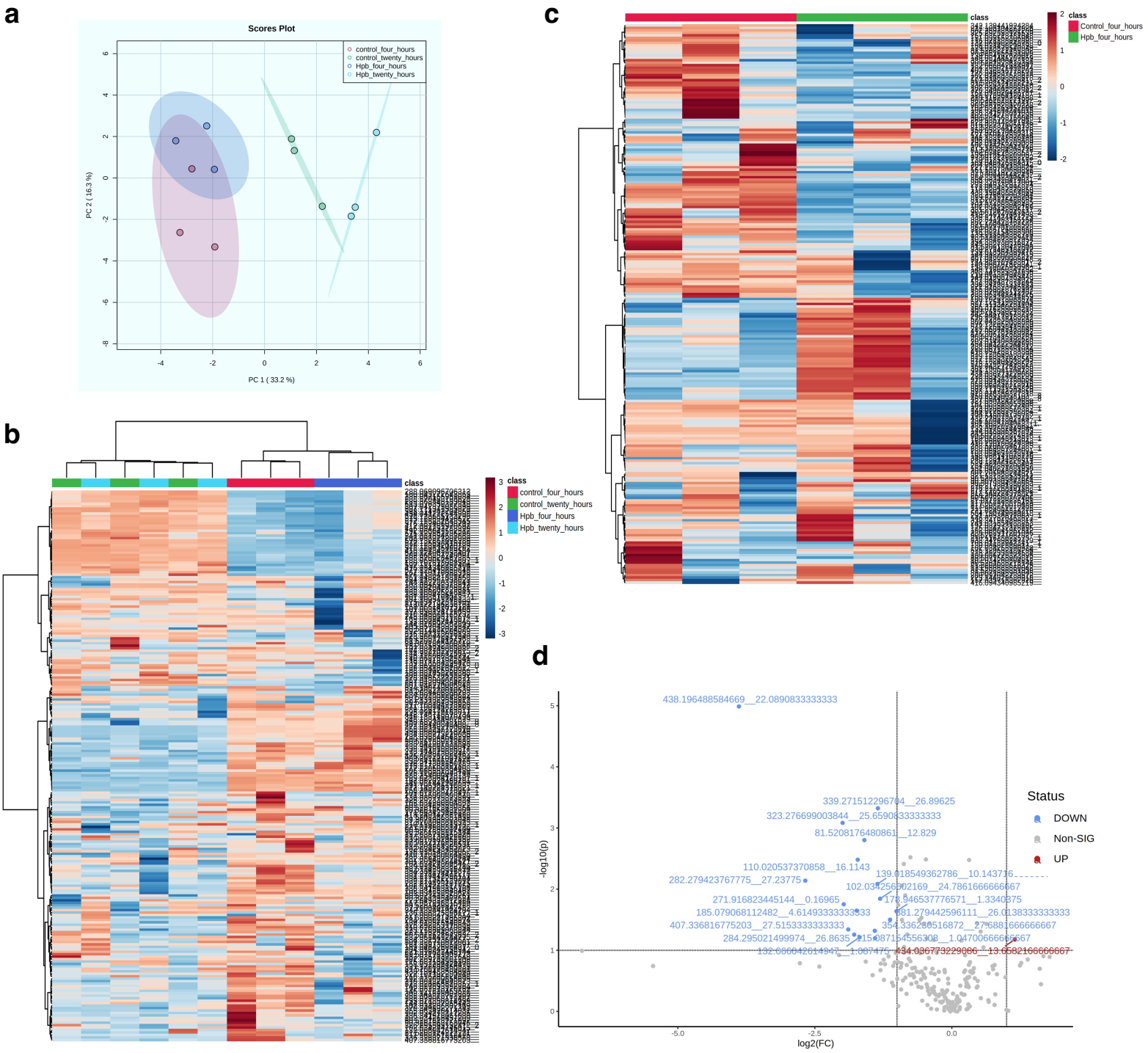

Supplementary Figure 1. Metabolomics and transcriptomics characterization of (HnpM)BMDCs at 4h and 20h. BMDCs were isolated and differentiated with 20ng/ml of GM-CSF. Cells were incubated with helminth-derived nonpolar metabolites for 4 and 20 h. The supernatants were collected, and metabolomics analysis was performed.

(a) Principal component analysis in which analysis was performed using the prcomp package. The calculation was based on singular value decomposition and the Rscript chemometrics.R is required. The 2-D scores plot between selected PCs is shown and the explained variances are given in brackets.

(b) Heatmap of all statistically enriched peak intensities. Red color represents metabolites with higher enrichment and blue for lower enrichment. The clustering was a result of distance measuring using Euclidean and clustering algorithm using ward.D.

(c) Heatmap of all statistically enriched peak intensities. Red color represents metabolites with higher enrichment and blue for lower enrichment. The clustering was a result of distance measuring using Euclidean and clustering algorithm using ward.D.

(d) Volcano plot. Important features selected by volcano plot with fold change threshold (x) 2 and t-tests threshold (y) 0.1. Both fold changes and p values were log transformed.

Supplementary Figure 2

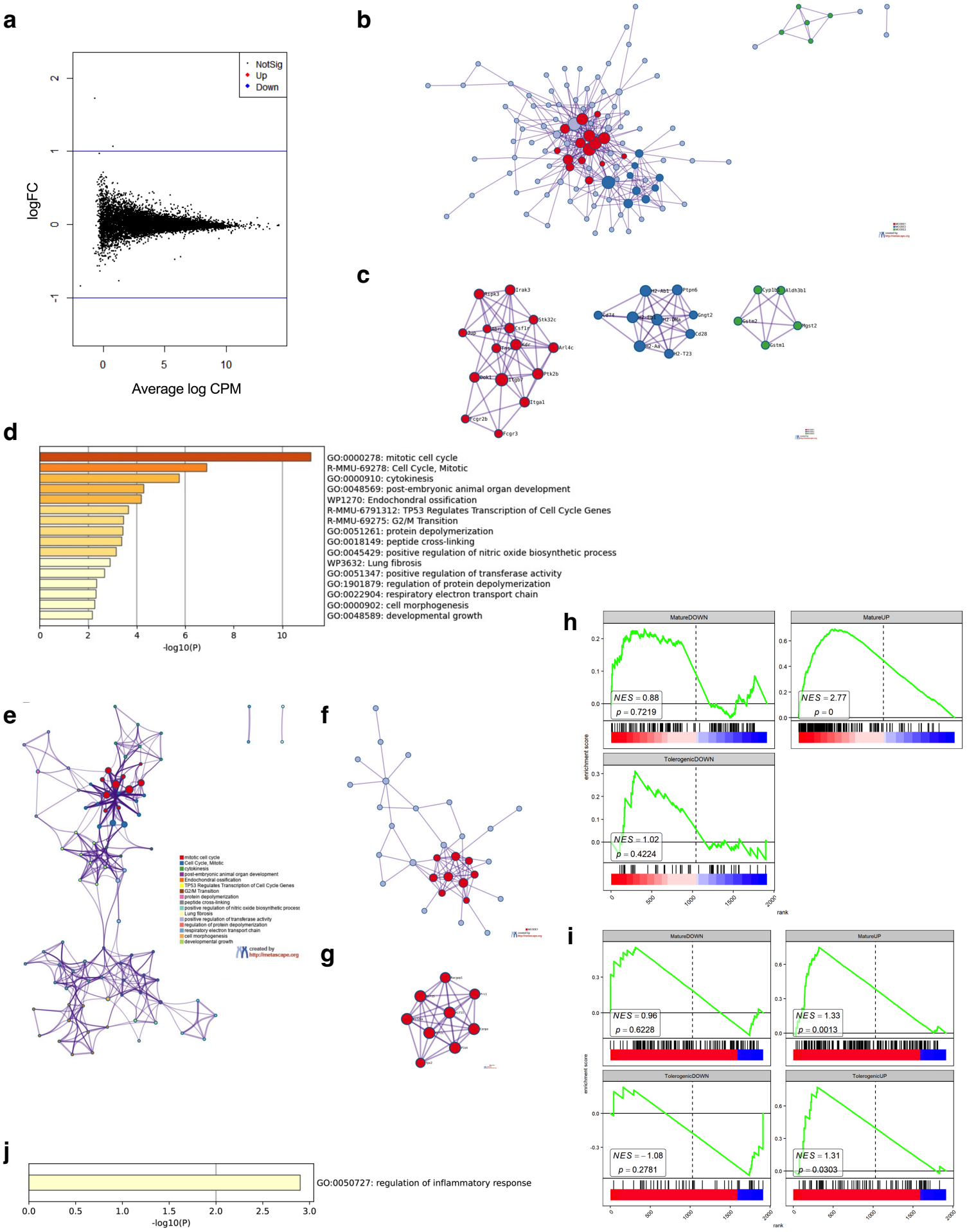

Supplementary Figure 2. Helminth-derived nonpolar metabolites induce a transcriptional signature in BMDCs

BMDCs were incubated with HnpM for 4 and 20h. The cell pellets were collected, mRNA was extracted with Trizol, and sequenced by Illumina RNA-seq Libraries, $n = 3$-4. Reads alignment and gene ID mapping were performed using Bowtie2 and HTSeq, respectively, against the Genome Reference Consortium Mouse Build 38 patch release 6 (GRCm38.p6) database.

(a) Volcano plot for gene expression at 4h. Read counts were obtained with Get_ReadCount.py and EdgeR with a likelihood test was performed to obtain differentially expressed genes. Genes were considered differentially expressed if the fold change ≥ 2 and $p \leq 0.05$.

(b) All protein-protein interactions among input genes were extracted from PPI data source and formed a PPI network.

(c) Network modules. Molecular complex detection (MCODE) algorithm was then applied to this network to identify neighborhoods where proteins are densely connected. MCODE1: GO:0046777|protein autophosphorylation|-6.6;GO:0043408|regulation of MAPK cascade|-6.4;GO:0006468|protein phosphorylation|-5.2; MCODE2: mmu05332|Graft-versus-host disease|-13.3;mmu05330|Allograft rejection|-13.3;GO:0019886|antigen processing and presentation of exogenous peptide antigen via MHC class II|-13.2; MCODE3: mmu00980|Metabolism of xenobiotics by cytochrome P450|-12.3;mmu00982|Drug metabolism - cytochrome P450|-9.2;mmu05204|Chemical carcinogenesis - DNA adducts|-8.9.

(d) Go annotation and pathway enrichment. All statistically enriched terms were identified based on the default choices under accumulative hypergeometric p-values and enrichment factors were calculated and used for filtering. Remaining significant terms were then hierarchically clustered into a tree based on Kappa-statistical similarities among their gene memberships. Then 0.3 kappa score was applied as the threshold to cast the tree into term clusters.

(e) Protein-protein interactions (PPIs) network among the input genes. A subset of representative terms from the full cluster was converted into a network layout and each term is represented by a circle node, where its size is proportional to the number of input genes fall under that term, and its color represent its cluster identity. Terms with a similarity score > 0.3 are linked by an edge and the thickness of the edge represents the similarity score.

(f) All protein-protein interactions among input genes were extracted from PPI data source and formed a PPI network.

(g) Network modules. Molecular complex detection (MCODE) algorithm was then applied to this network to identify neighborhoods where proteins are densely connected. MCODE1: R-MMU-983189|Kinesins|-13.8;R-MMU-6811434|COPI-dependent Golgi-to-ER retrograde traffic|-12.3;GO:0000226|microtubule cytoskeleton organization|-11.8.

(h, i) GSEA analysis, performed with phenoTest package in R. Gene sets were constructed with genes that are differentially expressed up and down. Gene sets were analyzed using published data on tolerogenic and inflammatory DCs (Supplementary File 5) Gene sets were represented using a barcode plot using the Limma package in R. **(h)** 20h and **(i)** 4h of incubation.

(j) Bar graph of enriched term across input gene lists**.** For each given gene list, pathway and process enrichment analysis has been carried out with the following ontology sources: GO Biological Processes, KEGG Pathway, Reactome Gene Sets, CORUM, TRRUST, PaGenBase and WikiPathways. All genes in the genome have been used as the enrichment background. Terms with a p-value < 0.01, a minimum count of 3, and an enrichment factor > 1.5 was collected and grouped into clusters based on their membership similarities. More specifically, p-values are calculated based on the cumulative hypergeometric distribution2, and q-values are calculated using the Benjamini-Hochberg procedure to account for multiple testing. Kappa scores4 are used as the similarity metric when performing hierarchical clustering on the enriched terms, and sub-trees with a similarity of > 0.3 are considered a cluster. The most statistically significant term within a cluster is chosen to represent the cluster.